Tone reversal patterning for advanced technology nodes

F. Schleicher, J. Bekaert, A. Thiam, S. Decoster, R. Blanc, et al.

F. Schleicher, J. Bekaert, A. Thiam, S. Decoster, R. Blanc, F. Lazzarino, J. Garcia Santaclara, G. Rispens, M. Maslow, "Tone reversal patterning for advanced technology nodes," Proc. SPIE 12056, Advanced Etch Technology and Process Integration for Nanopatterning XI, 1205605 (25 May 2022); doi: 10.1117/12.2610941

SPIE.

Event: SPIE Advanced Lithography + Patterning, 2022, San Jose, California, United States

Tone reversal patterning for advanced technology nodes

F. Schleicher*[a], J. Bekaert[a], A. Thiam[a], S. Decoster[a], R. Blanc[a], F. Lazzarino[a], J. Garcia Santaclara[b], G. Rispens[b], M. Maslow[b]

[a]IMEC, Kapeldreef 75, 3001 Leuven, Belgium
[b]ASML, De Run 6501, 5504 DR, Veldhoven, The Netherlands

ABSTRACT

As technology nodes continue to scale down, maintaining roughness and defectivity during the pattern transfer becomes more challenging. For the smallest features, Metal-Organic Resists (MOR) are preferred due to their better selectivity than Chemically Amplified Resists (CAR). However, MORs are usually negative tone resists. Primarily based on defectivity reasons, dark field Extreme Ultraviolet (EUV) masks are strongly preferred over light field EUV masks. Therefore, the MOR resist is more suited for pillar patterning than hole patterning. The purpose of this paper is to show that exposing pillars with MOR and converting them into holes can yield better roughness and defectivity than patterning holes with CAR directly. A similar comparison is done for the tone reversal of lines and spaces. It is shown that the Local Critical Dimension Uniformity (LCDU) of holes and the Line Edge Roughness (LER) of lines/spaces are well conserved throughout the tone inversion process.

Keywords: hole patterning, pillar patterning, lines and spaces, tone reversal, tone inversion, LER, dry etch, LCDU, EUV, metal-organic resist

1. INTRODUCTION

As the semiconductor industry requires increasingly more aggressive scaling, patterning materials also need to evolve. One of such evolutions is the switch in the Photoresist (PR) material, from Chemically Amplified Resists (CAR) to Metal-Organic Resists (MOR). MORs perform significantly better than CARs due to the presence of metallic particles, which results in better selectivity during etch processes compared to their non-metallic alternatives. Consequently, due to better selectivity, a thinner PR layer can be used which also helps to pattern features at very low dimensionsa thanks to a lower probability of pattern collapse after development.

However, MORs, unlike CARs, are of negative tone. This becomes an issue as for the Extreme Ultraviolet (EUV) lithography, dark field masks are preferred over light field masks due to contrast and defectivity performance. Consequently, MORs are suited more for pillar patterning, rather than hole patterning.

Since pillar patterning (MOR) will have better contrast and defectivity performance than hole patterning (CAR), in this work, we will pattern pillars using MOR, convert them into holes and compare if they perform better than holes patterned directly with CAR. We also compare results with the opposite scenario: we pattern holes with CAR and convert them into pillars (fig.1). In both cases, the study is performed on a hexagonal array of holes/pillars with a pitch of 46 nm x 80 nm (P46) and 40 x 70 nm (P40), and with the mask Critical Dimension (CD) of 24 nm and 26 nm. In parallel, we study the impact of the tone reversal on 28 nm and 26 nm pitch (P28, P26) MOR-patterned lines and spaces. Metrics of interest for the features studied are CD, Local CD Uniformity (LCDU, for pillars/holes), Line Edge Roughness (LER, for lines/spaces) and defectivity throughout the tone reversal process.

Advanced Etch Technology and Process Integration for Nanopatterning XI, edited by Julie Bannister, Nihar Mohanty, Proc. of SPIE Vol. 12056, 1205605
© 2022 SPIE · 0277-786X · doi: 10.1117/12.2610941

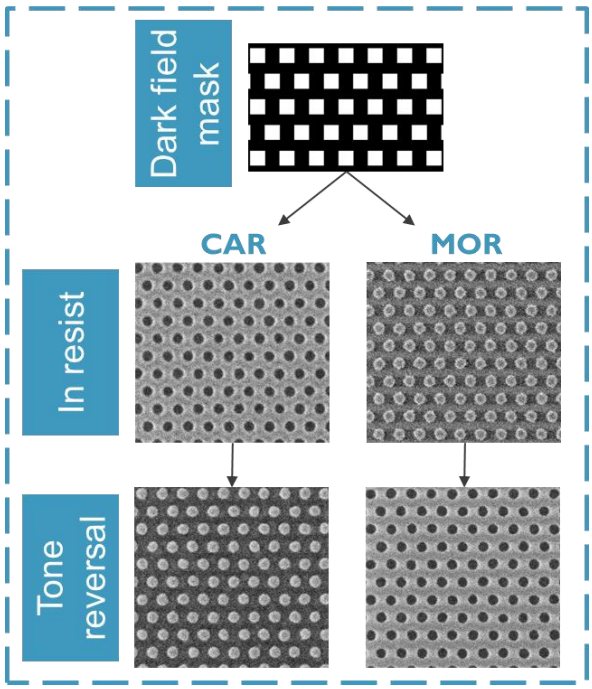

Figure 1. Illustrative picture of the experiment performed in this study. Dark field EUV mask is used to pattern holes using CAR and pillars using MOR. Afterwards, the tone reversal process converts these features into pillars and holes, respectively.

As will be discussed in detail in the methods section below, we have not decided to perform the tone inversion process by overcoating directly on the photoresist[1,2], but rather on an etched sacrificial layer below[3,4], as its height and shape can be tuned more easily than the profile of the photoresist. Moreover, it allows the tone inversion of multiple layers at once[5,6]. The Spin-on-Glass material has been chosen for the overcoat due to its well-understood planarization properties[7] and the in-house availability. Although the tone reversal of structures with similar dimensions has been reported using alternative materials[8,9], it is the first time that LCDU below 2 nm will be communicated.

2. TONE INVERSION OF CAR HOLES INTO PILLARS

2.1 Methods

The experiment is performed in the 300 mm IMEC facility, and the process flow is schematically shown on fig. 2. **Firstly**, the stack is deposited, and CAR is exposed so that holes are patterned in the resist. **Secondly**, the Spin-on-Glass (SoG) and the organic Advanced Patterning Film (APF) are open. Since APF and CAR are both organic materials, CAR is stripped during the APF etch step and SoG becomes the topmost layer in unpatterned regions on the wafer **Thirdly**, an additional SoG layer is spin-coated on the wafer, filling holes, and covering the initial SoG. **Finally**, this additional SoG is then etched back together with the original SoG, exposing APF and partially recessing the SoG into holes. The now exposed APF is then stripped and only SoG pillars (previously filling holes) remain standing. At this step, the tone inversion is complete.

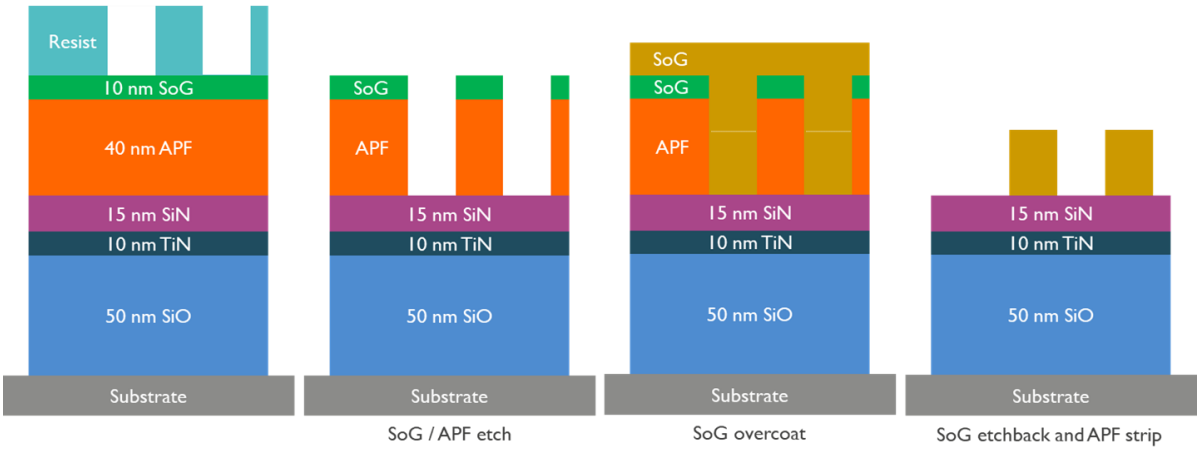

Figure 2. Process flow of tone inversion of CAR holes into pillars. 1. Stack deposition and PR exposure. 2. SoG and APF etch. 3. SoG overcoat and the level of the consecutive etch back indicated with the while line. 4. SoG etch back and APF strip.

As shown in Fig. 3, the level of the SoG etch back is difficult to estimate before the APF strip due to poor contrast of the SoG filling holes while the APF is still present. Once APF is stripped, 20 nm standing SoG pillars are clearly visible.

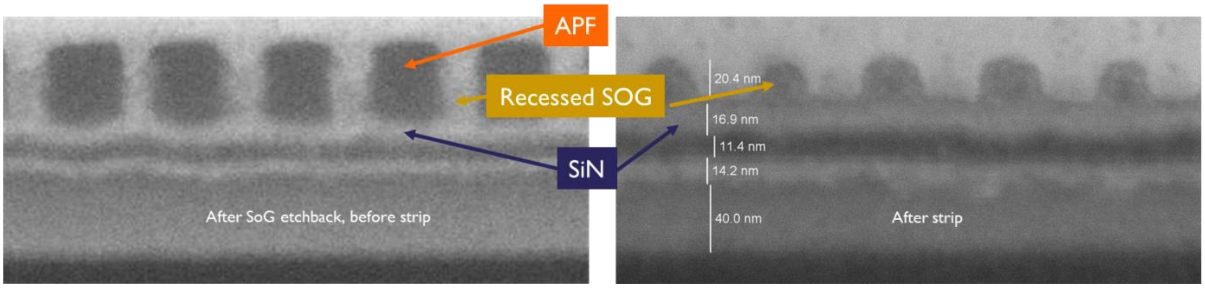

Figure 3. Focused Ion Beam (FIB) inspections of SoG pillars before (left) and after (right) APF strip at the end of the tone inversion process

2.2 Results

Quantitative results of the tone inversion of CAR P46 holes into pillars are shown on Fig.4 for three stages of the process: After Development Inspection (ADI, i.e. after exposure of CAR), After Etch Inspection (AEI, i.e. after SoG/APF etch) and finally After Tone Inversion (ATI). Illustrative pictures are complemented by the histogram with around 500k features measured. The initial ADI CD of 23 nm is well conserved AEI. However, LCDU goes significantly up, by 0.5 nm. This is attributed to the PR scum at the bottom of holes after exposure and development, which is not visible ADI, but affects the pattern transfer during the initial etch. This LCDU is relatively well-maintained ATI, but the measured CD of pillars goes up by 1.7 nm. This is most probably related to a small undercut in APF, which enlarges the hole CD and becomes the pillar CD at the end of the process. No defects like missing or merging pillars are found among all images.

Results for CAR P40 holes, shown on Fig. 5, are very similar to results for P46, except that LCDU is conserved slightly better, i.e. it goes up only by 0.2 nm AEI instead of 0.5 nm for P46. For this case, 678k features have been analyzed and only one potential defect has been found.

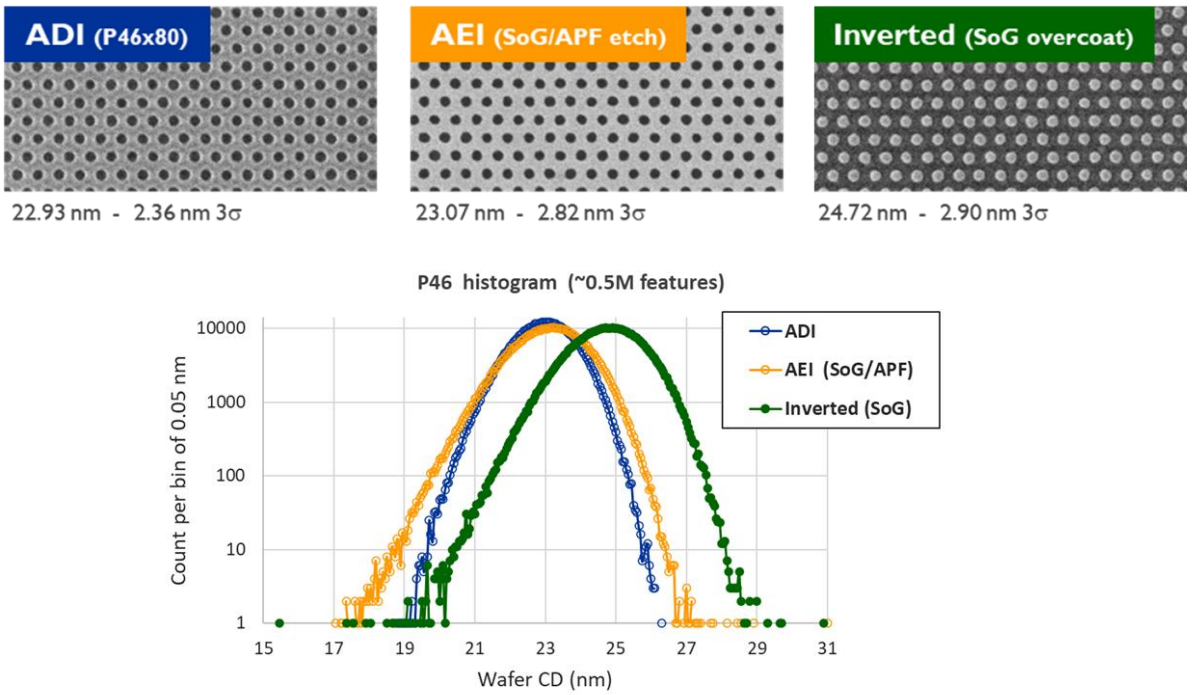

Figure 4. Summary (top) and detailed (bottom) results of the tone inversion of P46 holes into pillars.

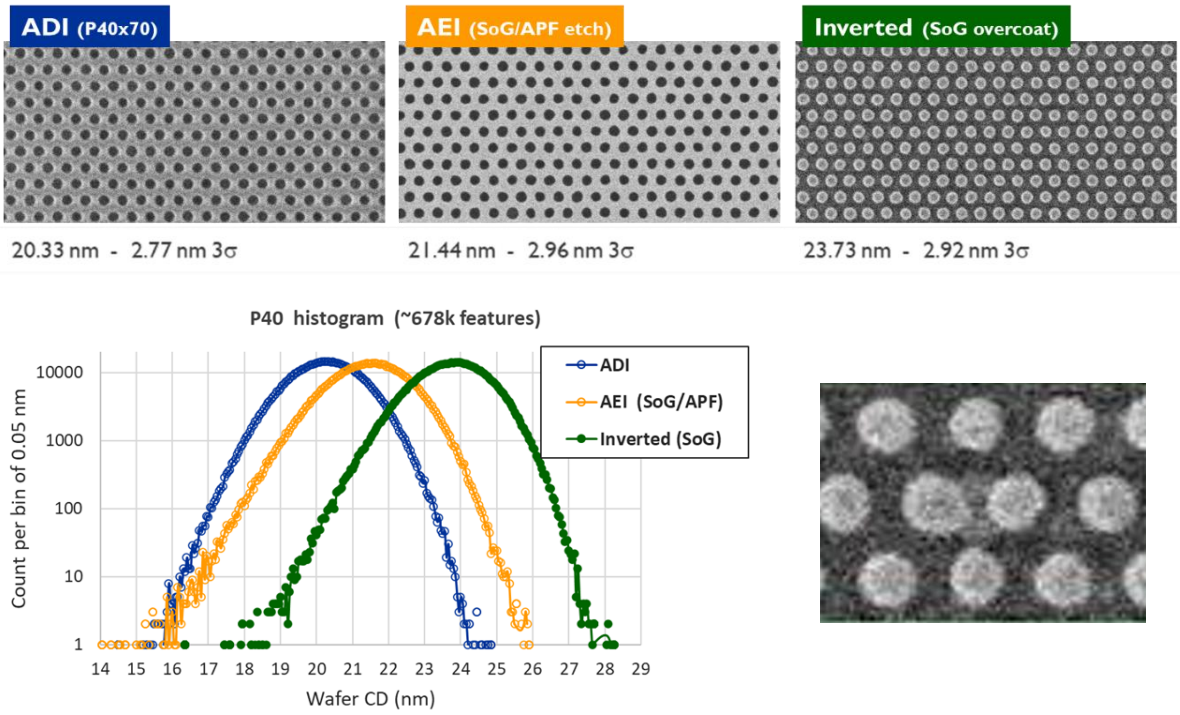

Figure 5. Summary (top) and detailed (bottom) ADI, AEI and ATI results of the tone inversion of P40 holes into pillars. Bottom right – the only merge-like defect found for P40 among 678k features analyzed.

In addition to dense arrays of holes/pillars discussed above, isolated features have also been measured. As shown on fig. 6, the etch back of SoG which results in 20 nm – 25 nm tall pillars on dense arrays, also allows to fully and clearly invert µm-sized patterns. However, for features larger than 6 µm residual SoG material is observed, and the tone inversion process cannot be completed. This is also the case for unpatterned regions of the wafer. As studied earlier[7], this behavior is a known limitation of spin-coated materials and is related to the local pattern density. Incorporation of dummy or density control features into the mask design could mitigate this issue.

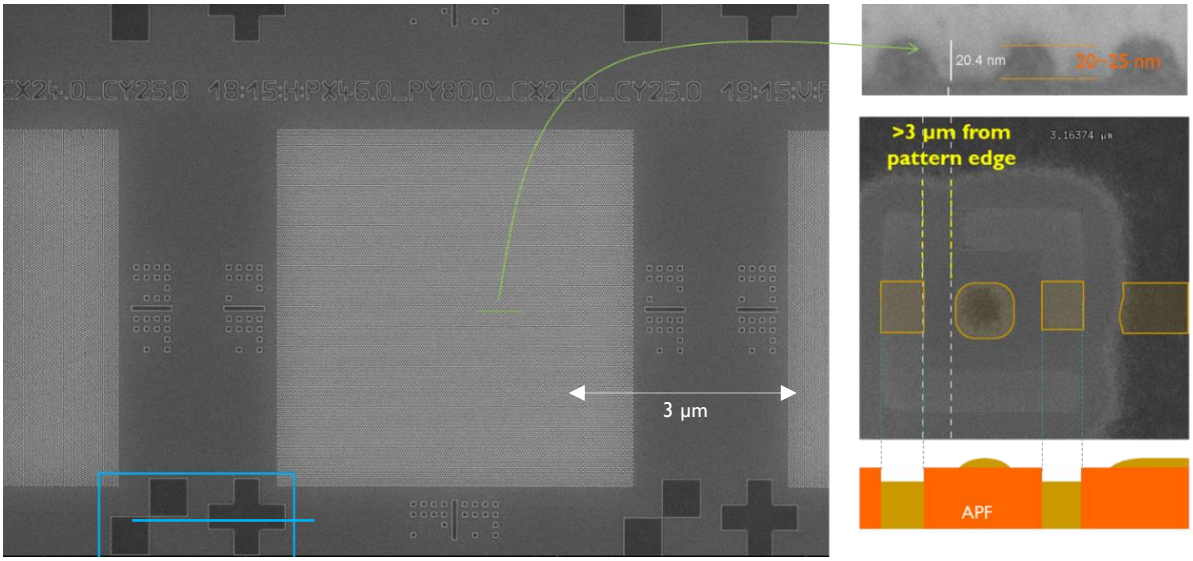

Figure 6. Successful tone inversion of CAR holes into pillars for the dense P46 array (green cut line and arrow) and for µm-sized patterns (blue frame). Unpatterned features 3 µm away from the pattern edge are not correctly inverted due to residual SoG remaining after the etch back (picture and schematic at the bottom right).

3. TONE INVERSION OF MOR PILLARS INTO HOLES

3.1 Methods

The initial process flow for tone inversion of MOR pillars into holes, which will be discussed in this section, is very similar to the one of the tone inversion of CAR holes into pillars (Fig. 7, top row). The only difference is the 65 nm thick SoC (Spin-on-Carbon) layer which is used instead of 35 nm of APF. Both materials behave very similarly from the etch process perspective.

Unlike the previous case, a patterning issue is observed in this experiment (Fig. 7, bottom row). Although the low LCDU of 2.00 nm is well preserved AEI, we observe a significant displacement of the patterned holes after tone inversion. The root cause of the displacement becomes evident with the FIB inspection after the SoG overcoat: SoC pillars become mechanically unstable and randomly slanted during this step, probably due to the stress induced by the SoG coating process, which also comprises of spinning, baking and solvent evaporation. Consequently, after SoG etch back and SoC strip, slanted holes remain on the wafer. By making the SoG etch back time shorter (longer) we end up with more (less) pattern displacement, since we then probe at higher (lower) SoG level where the effect of the taper is more (less) pronounced. However, since extension of the etch back would result in too much consumption of SoG and very shallow holes ATI, a liner-assisted stabilization of SoC pillars was attempted before the SoG overcoat. Figure 8 shows the adapted process flow with the 1.2 nm Atomic Layer Deposition (ALD) liner deposited on SoC pillar before the SoG overcoat. Due to the presence of the ALD liner, SoC pillars are now mechanically stabilized and protected from chemical processes during the overcoat. The post-deposition CD is 2.5 nm higher as expected, and LCDU is well conserved.

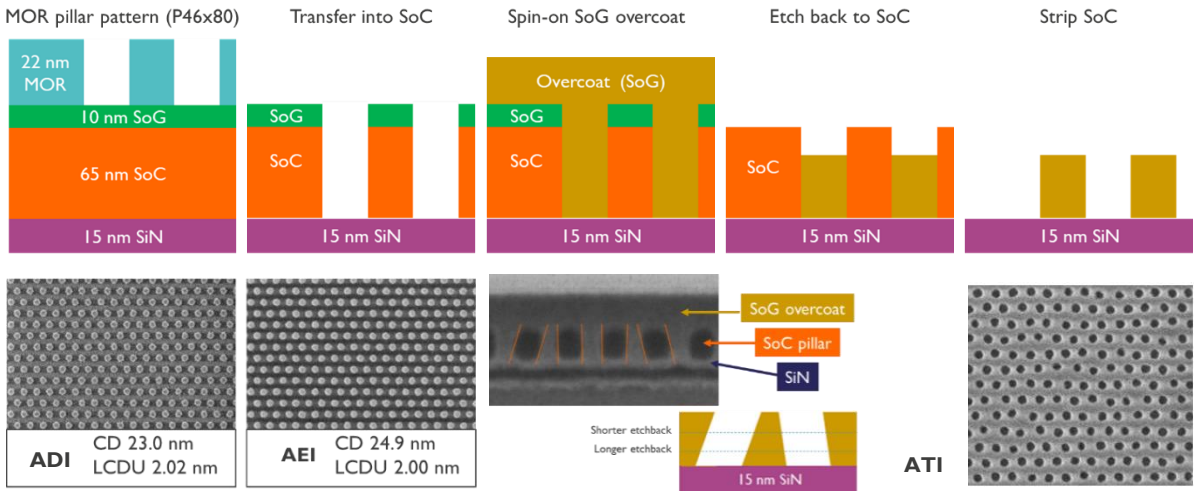

Figure 7. Top row: Initial process flow of tone inversion of MOR pillars into holes. Note only minor stack variations with respect to the previous case. Bottom row: Typical top-down inspections ADI, AEI and ATI, with cross-sectional FIB inspection after the SoG overcoat, when the SoC pillar instability is first observed. The schematic shows how more (less) taper/displacement is observed for shorter (longer) etch back. Inspections done on mask CD 24 nm.

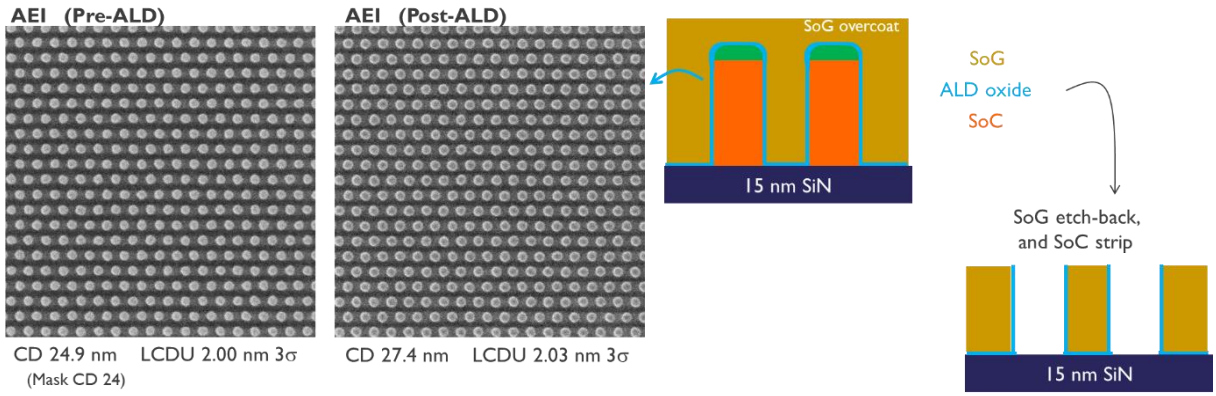

Figure 8. Adapted process flow of tone inversion of MOR pillars into holes. The 1.2nm ALD liner is deposited before the SoG overcoat, then removed from the top part together with the SoG during the etch back step. It will remain on sidewalls of holes after the SoC strip. Inspections done on mask CD 24 nm.

3.2 Results

Quantitative results of the tone inversion of MOR P46, mask CD 24 nm pillars into holes are shown in Fig.9 for three stages of the process. The initial ADI CD of 23 nm increased significantly after etch by almost 2 nm, still before the liner deposition. However, LCDU is well conserved at this step. After the liner deposition and the tone inversion process, CD is reduced well below the ADI value and LCDU goes up by only 0.3 nm. The reduction in CD is attributed to the undercut of the SoC pillar, not visible AEI due to the SoG cap which is still present. It is this reduced CD which is then transferred during the tone inversion process. Moreover, the O_2 precursor used during the ALD process trims the SoC pillar further. In order to evaluate the SoC CD below the SoG cap, a diluted HF has been applied after etch. Even though this caused most of the pillars to fall, around 100 remaining standing SoC pillars without the SoG cap could be measured. They indeed turned out to be 1.2 nm smaller. It has to be noted that these remaining standing pillars are usually the largest ones, so the average global trim could be larger.

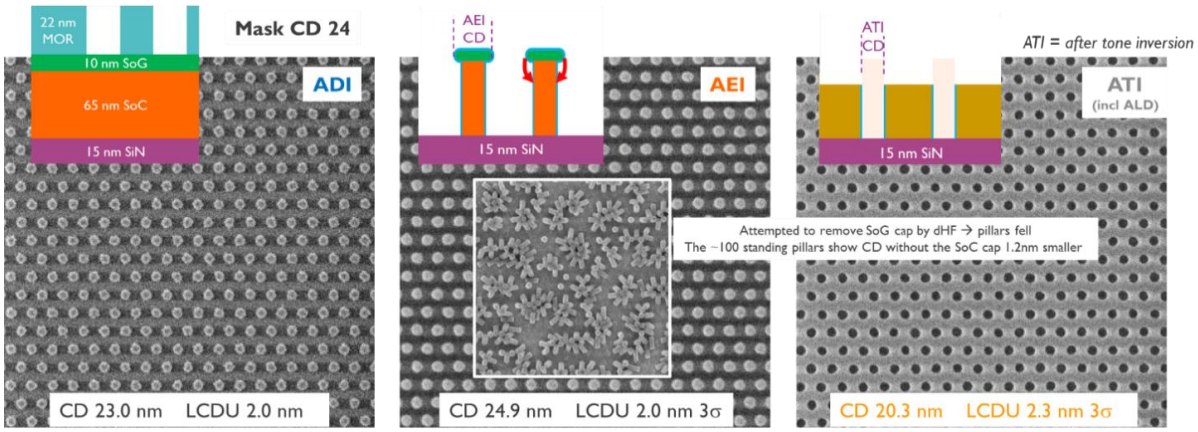

Figure 9. Summary of results of the tone inversion of P46 holes into pillars for the mask CD 24 nm. Schematic of the SoC trim after etch is also shown, together with the diluted HF experiment results and the few remaining standing pillars measured. The reduced ATI CD is the direct consequence of the SoC trim after etch.

Fig. 10 shows results of the same process on P46 features but with a mask CD of 26 nm. Similarly to the 24 nm case, we observe a CD increase after etch and a CD reduction after tone inversion. However, for this larger mask CD we note that the initial LCDU 1.9 nm is well conserved throughout the entire process and remains at 1.9 nm ATI. While the process could be fine-tuned in order to reduce the CD variation ADI/AEI/ATI, we see no fundamental showstoppers for application at larger or smaller pitches.

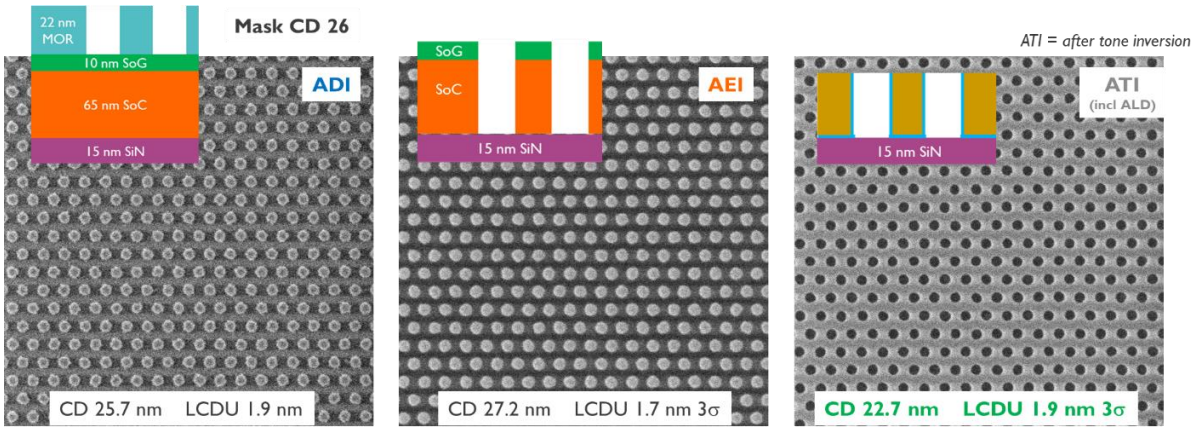

Figure 10. Summary of results of the tone inversion of P46 holes into pillars for the mask CD 26 nm. Note the very low LCDU ADI is conserved throughout the entire tone reversal process.

Similarly to the CAR holes into pillar scenario (Fig.6), we have also performed measurements of isolated features. As shown on Fig. 11, µm-sized patterns are also fully and clearly inverted. Moreover, the cross section of the dense array shows that the etch back of SoG results in 20 nm – 25 nm deep holes on dense arrays.

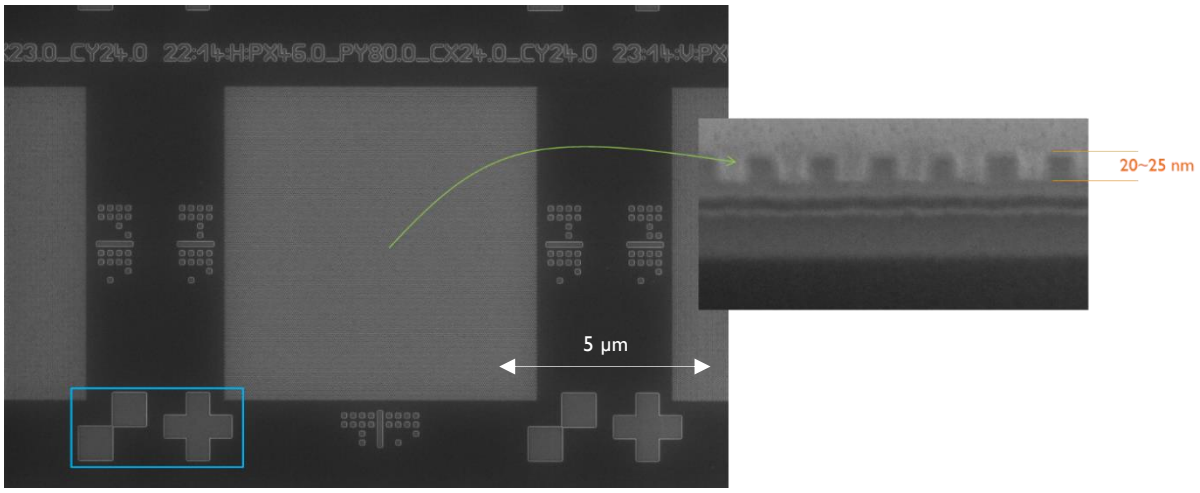

Figure 11. Tone inversion of the dense array of MOR pillars into holes results in 20 nm – 25 nm deep holes (green arrow). µm-sized patterns (blue box) are also fully and clearly inverted.

4. TONE INVERSION OF MOR LINES/SPACES INTO SPACES/LINES

4.1 Methods

The final part of the paper discusses the tone inversion of MOR lines/spaces into spaces/lines. The flow is similar to the previously discussed cases, except that here a 40 nm thick APF layer is used (Fig.12). Thanks to this material, thinner and stronger than SoC, no ALD liner had to be used in order to stabilize structures. Moreover, due to the reduced stack thickness, thinner SoG overcoat is needed (56 nm in total, instead of 80 nm in the previous case), which reduces the stress impact on APF. Furthermore, lines and spaces are naturally mechanically stable than pillars.

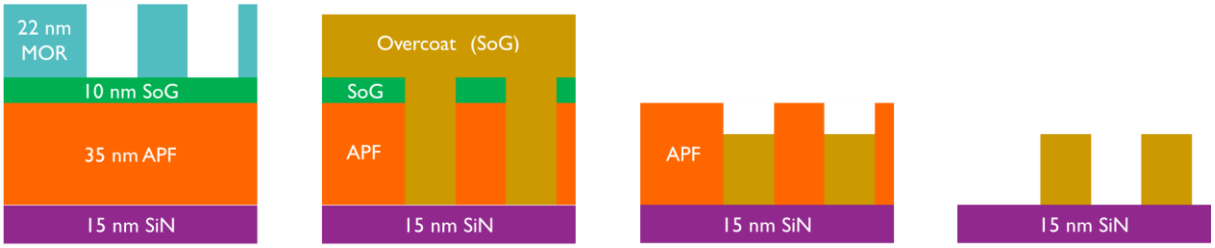

Figure 12. Process flow of tone inversion of MOR lines and spaces.

4.2 Results

Illustrative and CD results of the tone inversion on lines and spaces of pitch 26 nm and 28 nm are shown in Fig. 13. In both cases the tone inversion is indeed successful. We see that the CD variation AEI to ATI is limited, with only 1 nm of difference AEI to ATI for both pitches.

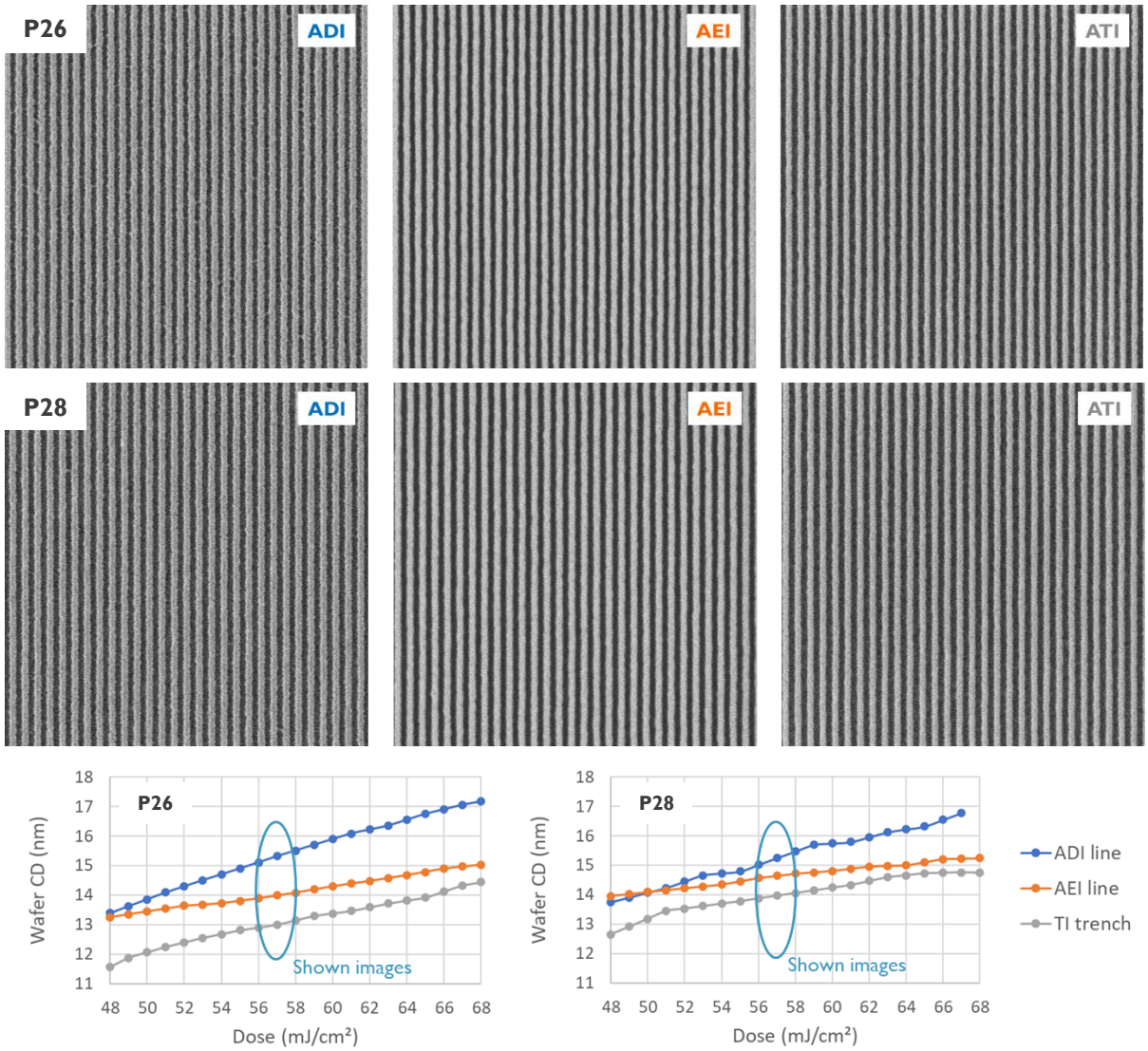

Figure 13. Illustrative and CD results of the tone inversion process on lines and spaces of pitch 26 nm and 28 nm.

The detailed analysis of the results, performed using the Fractilia™ MetroLER software, is shown on Fig. 14. For both pitches, the roughness is significantly improved from ADI to AEI. Please note that as ATI lines become spaces and vice versa, line width roughness (LWR) ATI is compared to space width roughness (SWR) AEI. The main difference is in low (long-range) frequencies, where the roughness ATI is slightly higher than AEI. This is also visible in the increase in LER ATI and it is attributed to a non-negligible amount of stress induced by the overcoat process. Findings for both pitches are very similar, except for the 0.2 nm lower roughness in the P28 case, due to the lower roughness after development for a more relaxed pitch.

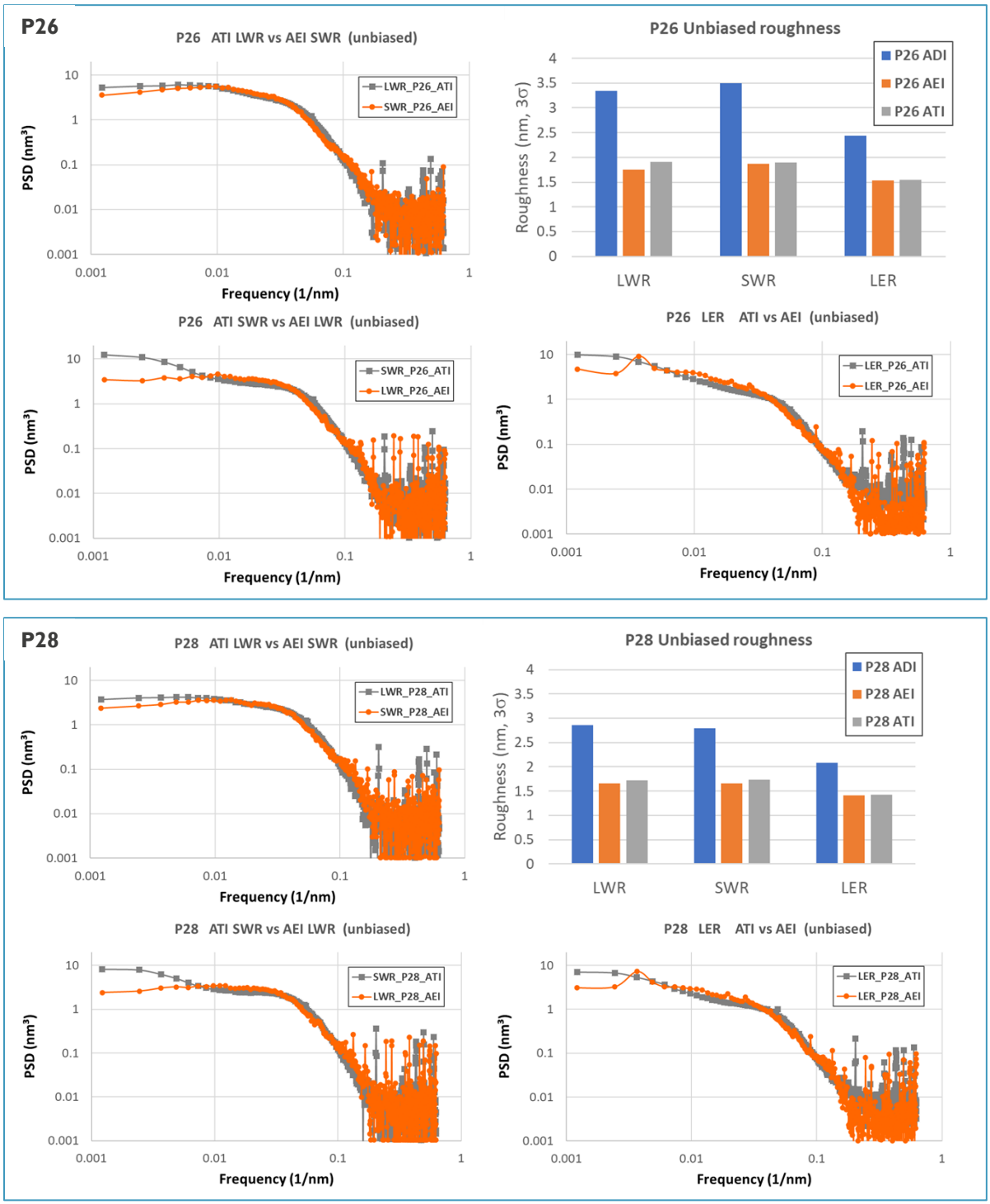

Figure 14. Detailed results of the tone inversion process on lines and spaces of pitch 26 nm (top panel) and 28 nm (bottom panel): Unbiased power spectral density (PSD) comparison for ATI LWR vs AEI SWR (top-left), ATI SWR vs AEI LWR (bottom-left), ATI vs AEI LER (bottom-right) and evolution of unbiased roughness for all three inspection steps (top-right).

Similarly to the previous case of MOR pillars inverted into contacts, we also see that that large features are clearly and fully inverted (Fig. 15).

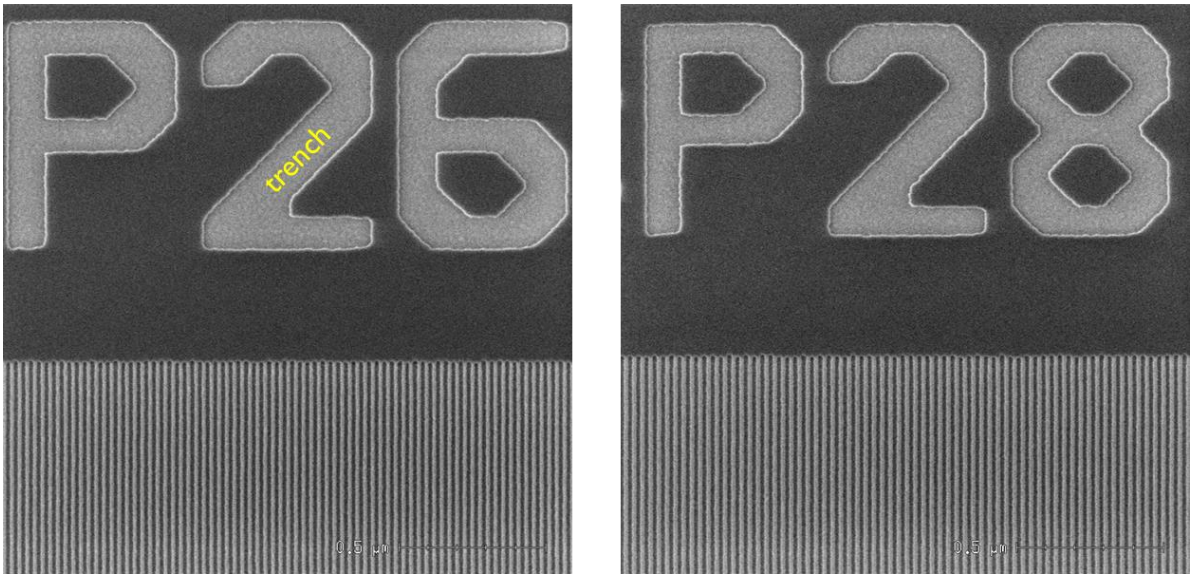

Figure 15. Successful tone inversion of µm-sized patterns next to the dense array of lines and spaces.

Unlike for contacts and pillars, FIB resolution would not allow to precisely measure the SoG spaces ATI and the TEM inspection of lines and spaces has been performed after the tone inversion process (Fig. 16). We note that for P26 lines and spaces 22 nm of SoG remains, which is in line with our findings for pillars and holes.

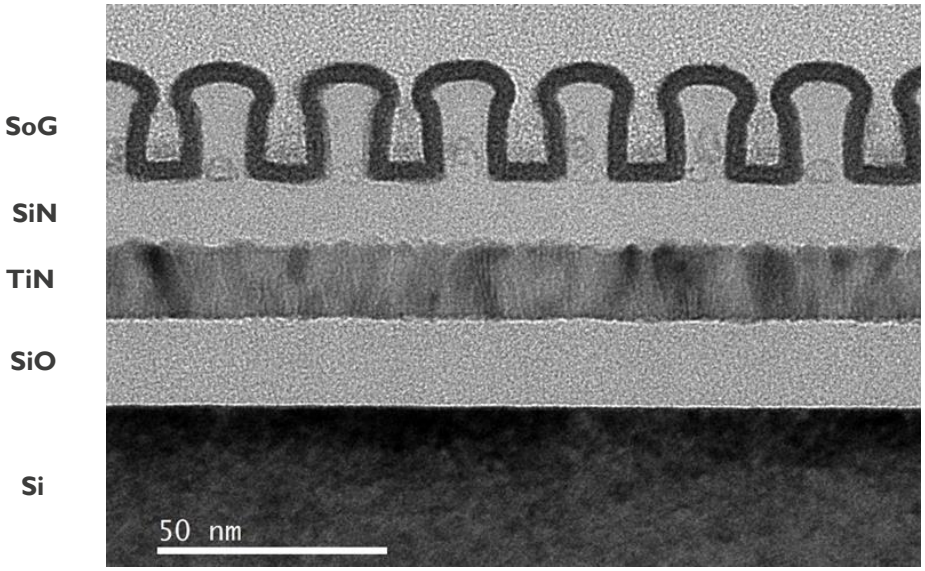

Figure 16. TEM inspection of P26 lines and spaces ATI showing 22 nm of SoG remaining.

In agreement with a previous study[10], breaks in MOR lines are very rare. In this work we indeed find only bridge defects ADI and AEI, which consequently become breaks ATI. Relatively large number of bridge detections ADI (2 per SEM image for P26) is strongly reduced after etch - we observe only a few defects per 500 SEM images, which translates to less than 1 defect per mm (Fig. 17). Due to the very low amount of defects detected, both P26 and P28 results look comparable, while the real total number of defects is expected to be somewhat higher for the P26 case, due to the more agressive pitch.

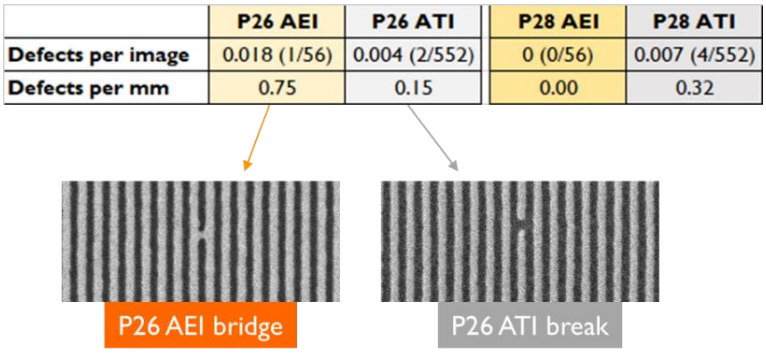

Figure 17. Defect analysis of P26 and P28 lines and spaces AEI and ATI, together with an illustration of a typical P26 bridge defect AEI becoming a break ATI.

In addition to P28 and P26 lines and spaces, we preliminarely demonstrate that the process is also possible on agressive P24 (Fig. 18). While this may be the performance limit of the process and while we detect several defects ADI, AEI and ATI, we nevertheles observe that LWR is significantly reduced AEI and ATI with respect to ADI. As the SoG etch back process could be further tuned for P24, we expect even lower defectivity possible.

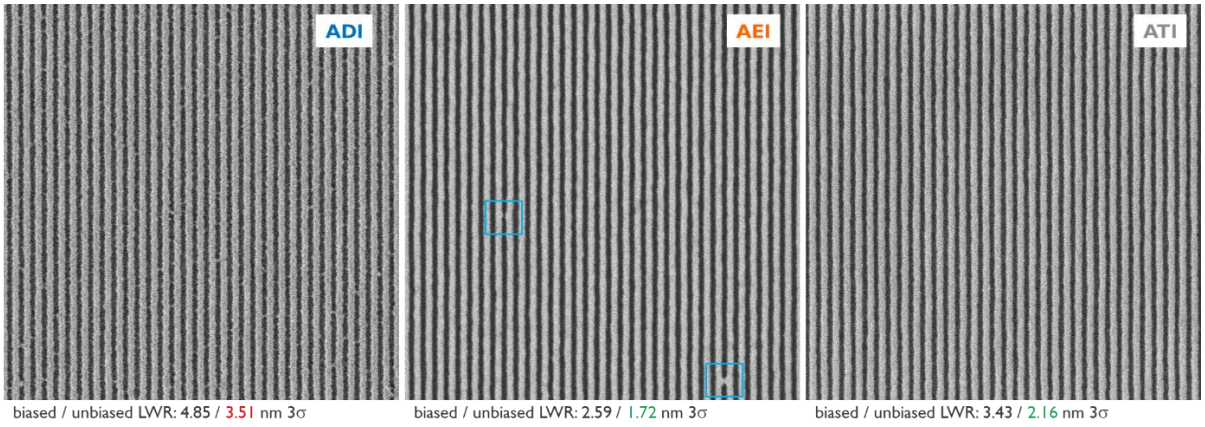

Figure 18. Illustrative results of the tone inversion process on lines and spaces of pitch 24 nm, together with LWR values associated. Blue boxes point to bridge defects detected AEI.

5. CONCLUSIONS

In conclusion, we have successfully applied the tone inversion on three different types of patterns with aggressive dimensions: 1) CAR holes into pillars; 2) MOR pillars into holes and 3) MOR lines/spaces into spaces/lines. In case of MOR pillars conversion into holes, the ALD oxide liner had to be used in order to stabilize pillars and prevent the pattern displacement. All three options resulted in the clean and complete inversion of the pattern up to µm-sized features with very low defectivity. Importantly, in case of MOR-based features, the initial LCDU/LER improves significantly after the initial etch and remains low throughout the tone reversal process. Moreover, the tone inverted MOR pillars provide significantly better LCDU compared to holes printed directly with CAR. Therefore, the tone inversion process provides a viable patterning alternative, even for aggressive dimensions: Instead of directly patterning holes with CAR, one can pattern MOR pillars then convert them into holes for significantly improved LCDU performance.

ACKNOWLEDGEMENTS

Authors would like to acknowledge the IMEC pilot line for the processing.

REFERENCES

[1] David J. Abdallah, Kazunori Kurosawa, Elizabeth Wolfer, Victor Monreal, M. Dalil Rahman, DongKwan Lee, Mark Neisser, Ralph R. Dammel, "Image reversal trilayer materials and processing," Proc. SPIE 7520, 75200L (2009).
[2] Niyaz Khusnatdinov, Gary Doyle, Douglas J. Resnick, Zhengmao Ye, Dwayne LaBrake, Brennan Milligan, Fred Alokozai, Jerry Chen, "Development of a robust reverse tone pattern transfer process," Proc. SPIE 10146, 101461A (2017).
[3] Chi-Chun Liu, *et al.*, "Exploration of pillar local CDU improvement options for AI applications (Conference Presentation)," Proc. SPIE 11326, 113260W (2020).
[4] V. M. Blanco Carballo, *et al.*, "Single exposure EUV of 32nm pitch logic structures: patterning performance on BF and DF masks," Proc. SPIE 10583, 105830L (2018).
[5] Angélique Raley, Nihar Mohanty, Xinghua Sun, Richard A. Farrell, Jeffrey T. Smith, Akiteru Ko, Andrew W. Metz, Peter Biolsi, Anton Devilliers, "Self-aligned blocking integration demonstration for critical sub-40nm pitch Mx level patterning," Proc. SPIE 10149, 101490O (2017).
[6] V. Vega-Gonzalez *et al.*, "Three-Layer BEOL Process Integration with Supervia and Self-Aligned-Block Options for the 3 nm Node," 2019 IEEE International Electron Devices Meeting (IEDM), 19.3.1 (2019).
[7] Stefan Decoster, Xiaoyu Piao, Werner Gillijns, and Frédéric Lazzarino, "Modeling the topography of uneven substrates post spin-coating", Journal of Vacuum Science & Technology B 36, 03E102 (2018).
[8] Shuhei Shigaki, Wataru Shibayama, Satoshi Takeda, Mamoru Tamura, Makoto Nakajima, Rikimaru Sakamoto, "DDR process and materials for novel tone reverse technique," Proc. SPIE 10583, 105830M (2018).
[9] Yasushi Sakaida, Hiroaki Yaguchi, Rikimaru Sakamoto, Bang-Ching Ho, "Development of reverse materials for double patterning process," Proc. SPIE 7639, 76391Z (2010).
[10] D. De Simone, *et al.*, "28nm pitch single exposure patterning readiness by metal oxide resist on 0.33NA EUV lithography," Proc. SPIE 11609, 116090Q (2021).